Electronic Supplementary Material (ESI) for Nanoscale.

Supplementary Material

Identification and Optimization of Tunable Endosomal Escape Parameters for Enhanced Efficacy in Peptide-Targeted Prodrug-Loaded Nanoparticles

Franklin Mejia[a], Sabrina Khan[a], David T. Omstead[a], Christina Minetos[a] & Basar Bilgicer[a,b,c,d]*

[a] Department of Chemical and Biomolecular Engineering, University of Notre Dame, Notre Dame, IN 46556

[b] Department of Chemistry and Biochemistry, University of Notre Dame, Notre Dame, IN 46556

[c] Harper Cancer Research Institute, University of Notre Dame, Notre Dame, IN 46556

[d] Advanced Diagnostics and Therapeutics, University of Notre Dame, Notre Dame, IN 46556

*Address correspondence to Prof. Basar Bilgicer, University of Notre Dame, 205C McCourtney Hall, Notre Dame, IN, 46556-5637. E-mail: bbilgicer@nd.edu.

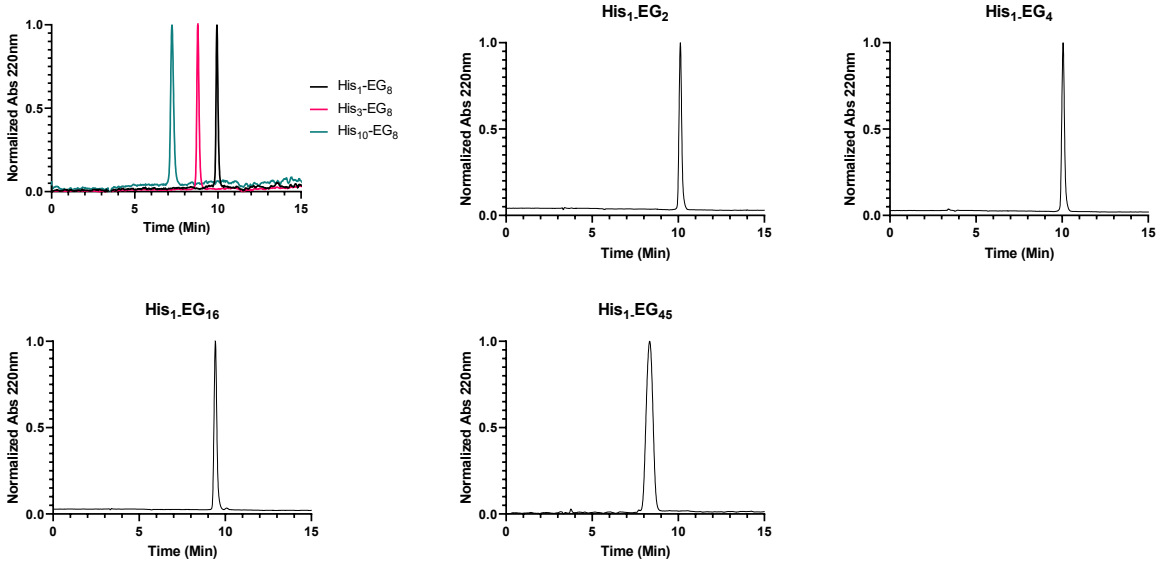

Supplementary Figure S1. Purity of His_n-EG_m conjugates was confirmed by RP-HPLC (>90%) using a Zorbax C3 semiprep column and a 2-propanol/acetonitrile/water gradient.

Supplementary Table S1. QTOF Mass Spectrometry Analysis of His_n-EG_m lipid conjugates confirms identity of His_n-EG_m conjugates.

Molecule	Expected Mass (Da)	Observed Mass (Da)
His_1-EG_2	1103.8	1103.8
His_1-EG_4	1191.9	1191.9
His_1-EG_8	1368.0	1368.0
His_1-EG_{16}	1791.2	1792.2
His_1-EG_{45}	2982.9	2983.9
His_3-EG_8	1642.1	1643.1
His_{10}-EG_8	2601.5	2602.5

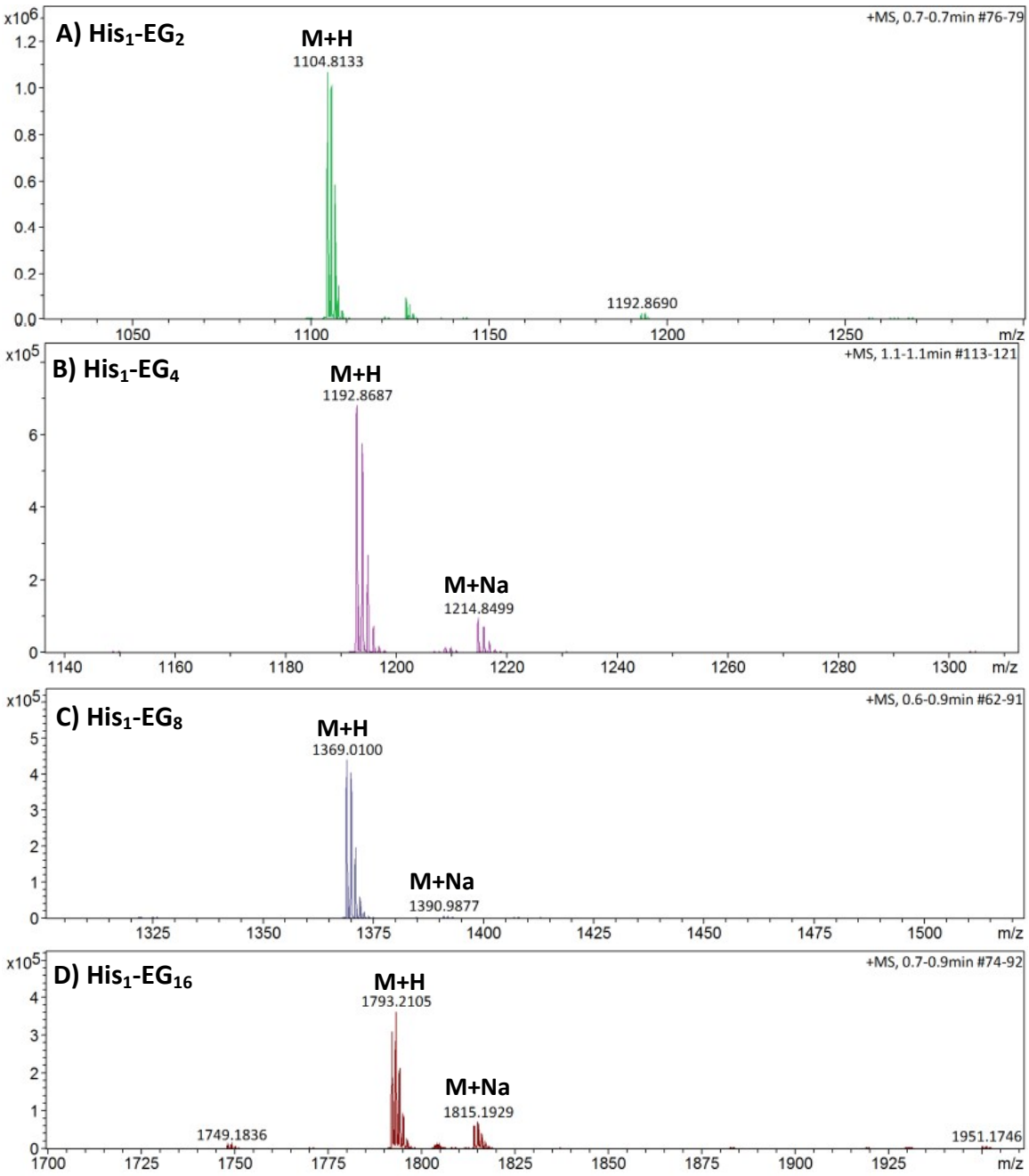

Supplementary Figure S2 (Continued on page S4). Mass Spectra of His_n-EG_m conjugates was obtained by QTOF MS. A) His_1-EG_2, B) His_1-EG_4, C) His_1-EG_8, D) His_1-EG_{16}, E) His_1-EG_{45}, F) His_3-EG_8, G) His_{10}-EG_8.

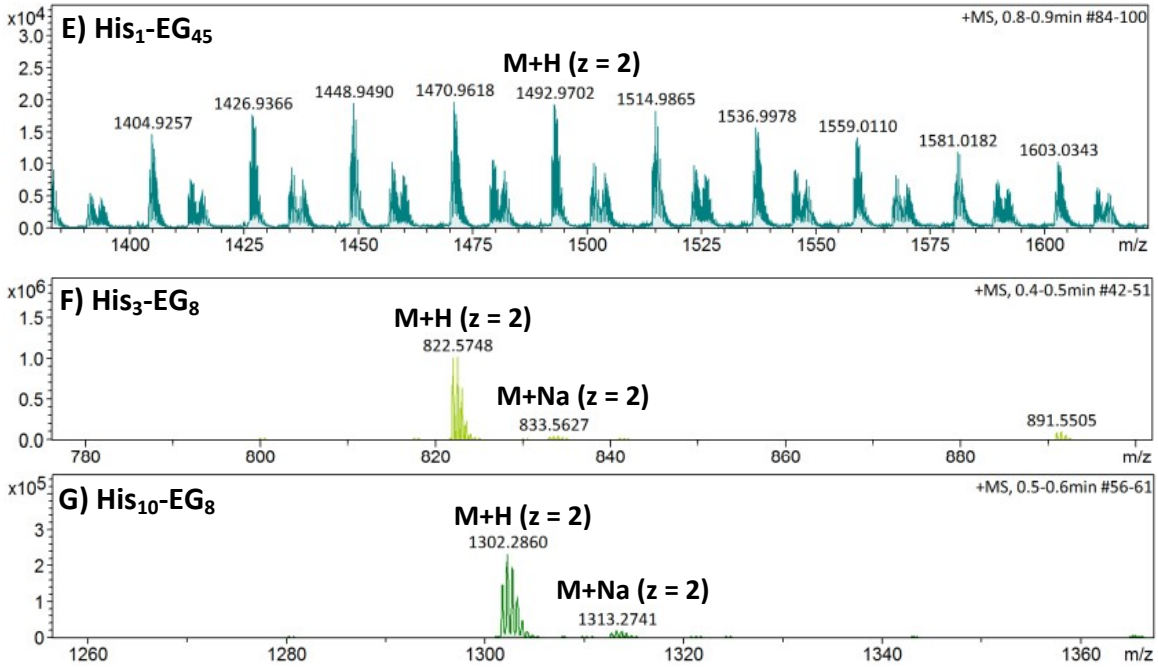

Supplementary Figure S2 (Continued). Mass Spectra of His_n-EG_m conjugates was obtained by QTOF MS. A) His_1-EG_2, B) His_1-EG_4, C) His_1-EG_8, D) His_1-EG_{16}, E) His_1-EG_{45}, F) His_3-EG_8, G) His_{10}-EG_8.

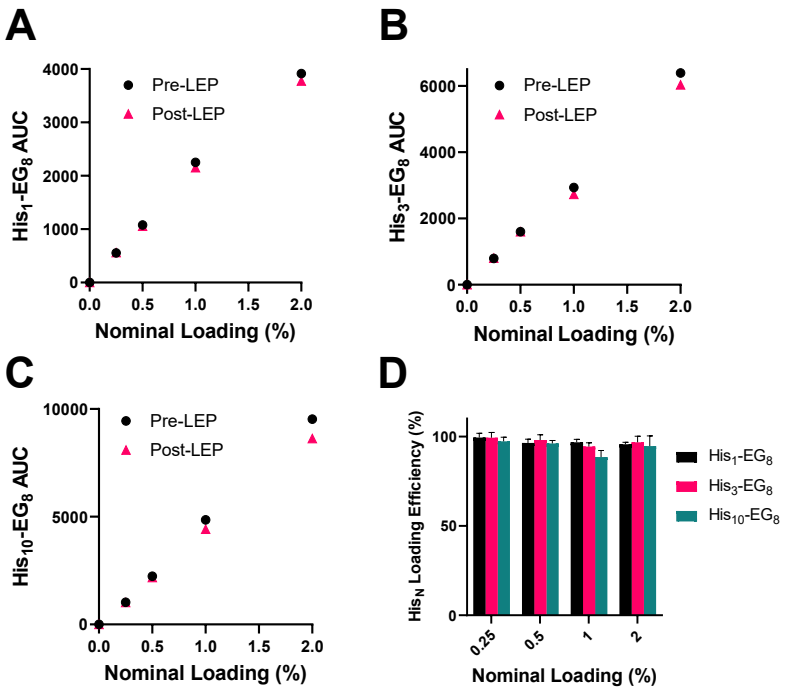

Supplementary Figure S3. Loading efficiency of His_n-EG_8 onto NP was analyzed using a Zorbax C3 semiprep column and a 2-propanol/acetonitrile/water gradient.

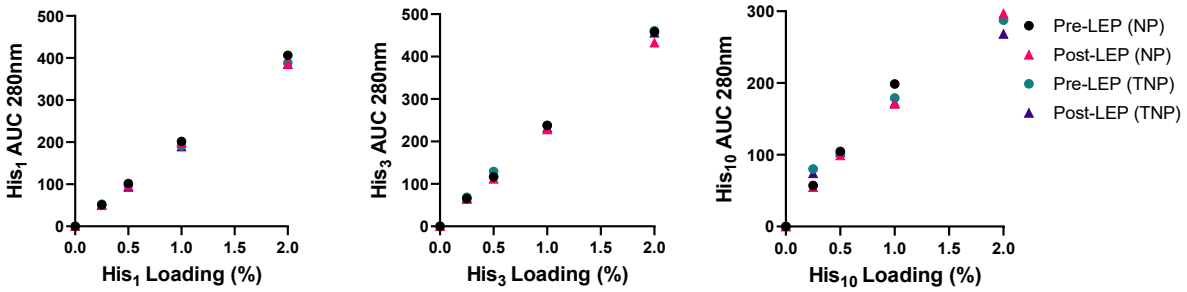

Supplementary Figure S4. Loading efficiency of His_n-EG_8 onto TNP was His_n content in NP and TNP was compared and confirmed to be equivalent.

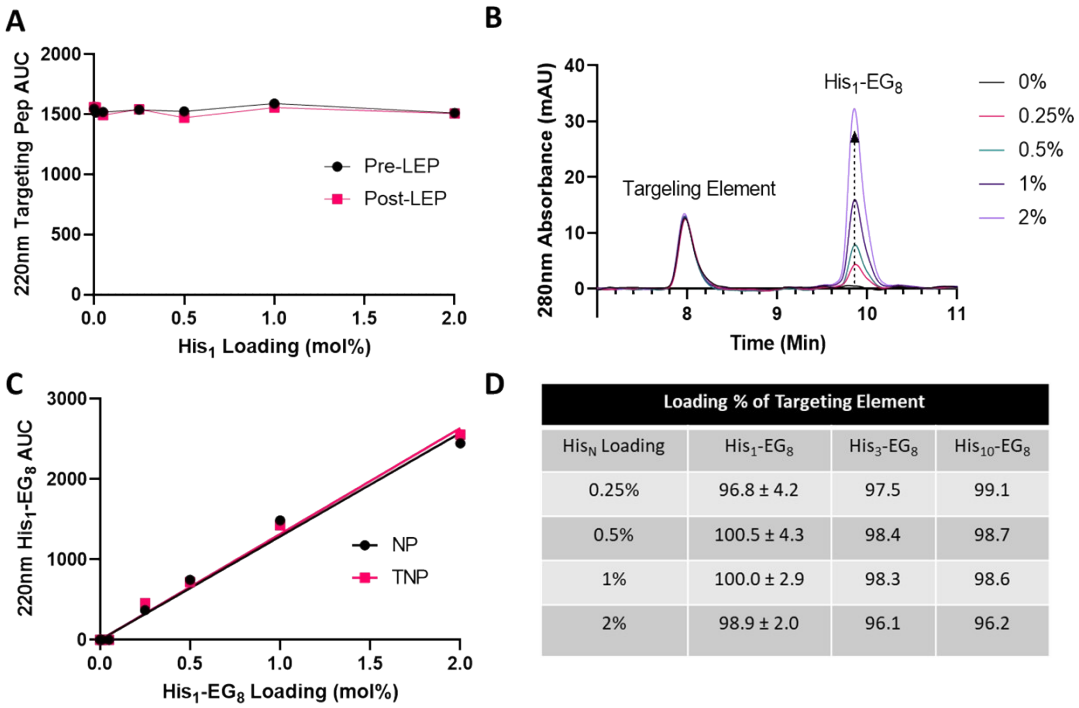

Loading % of Targeting Element			
His_N Loading	His_1-EG_8	His_3-EG_8	His_{10}-EG_8
0.25%	96.8 ± 4.2	97.5	99.1
0.5%	100.5 ± 4.3	98.4	98.7
1%	100.0 ± 2.9	98.3	98.6
2%	98.9 ± 2.0	96.1	96.2

Supplementary Figure S5. The effect of His_n-EG_8 on the loading of targeting elements was evaluated up to 2% mol of His_n-EG_8 at a constant 1% mol of targeting peptide-lipid conjugate and analyzed using a Zorbax C3 semiprep column and a 2-propanol/acetonitrile/water gradient.

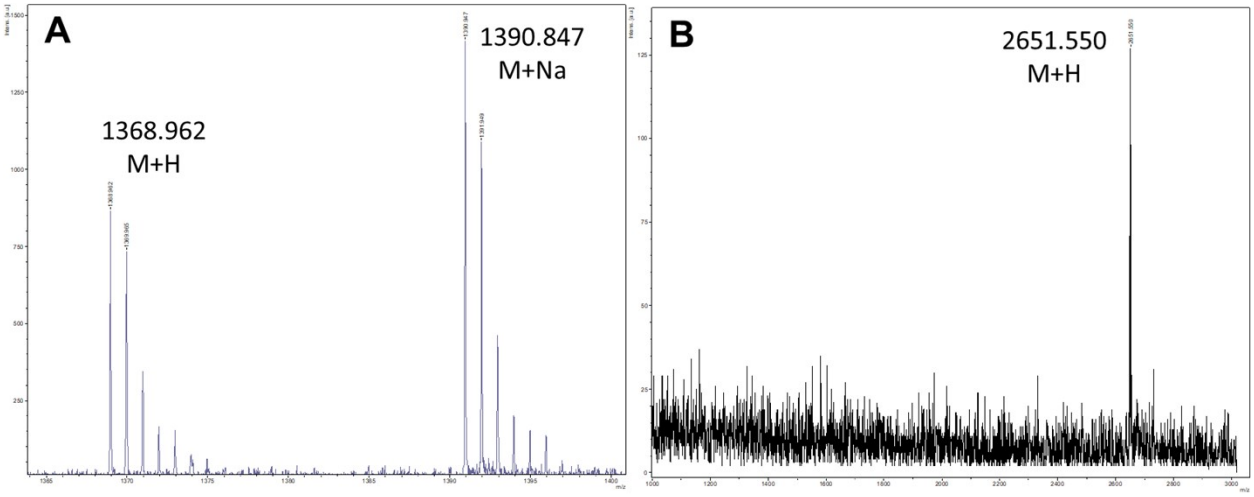

Supplementary Figure S6. His_1-EG_8 LPAM1pep TNP were synthesized, purified by liposomal extruder purification (LEP) to remove unincorporated compounds and analyzed by RP-HPLC. His_1-EG_8 and LPAM1pep fractions were collected and analyzed by MALDI MS to confirm preservation of the compounds throughout the nanoparticle synthesis process. His_1-EG_8 expected: 1368.0, found: 1368.962 (M+H), 1390.847 (M+Na). LPAM1pep expected: 2650.6, found: 2561.55 (M+H).

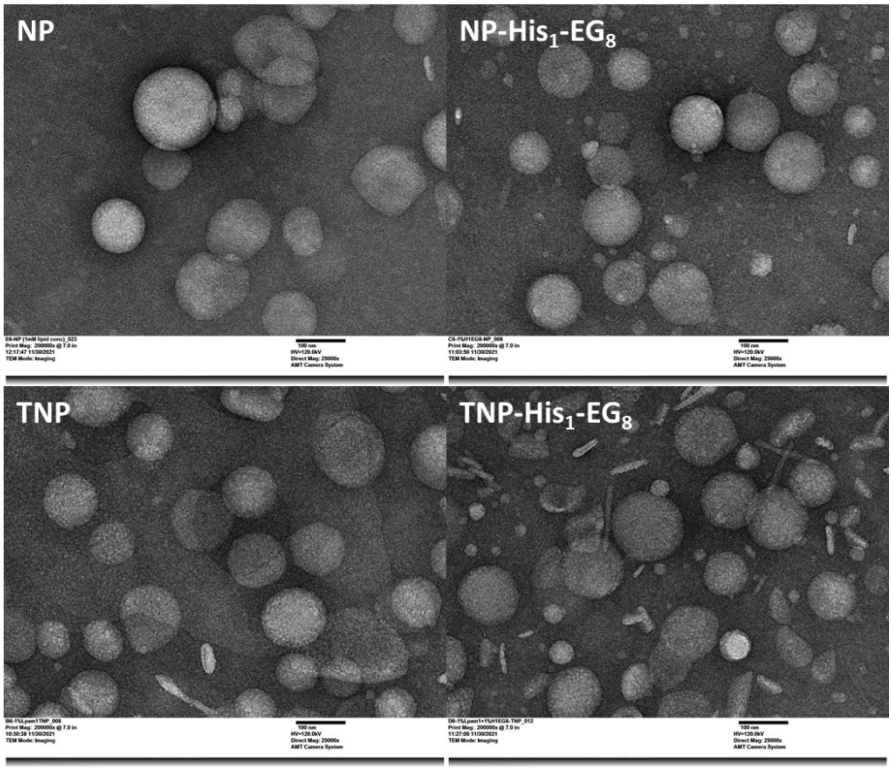

Supplementary Figure S7. Transmission Electron Microscopy images of NP and TNP with and without His_1-EG_8 show nanoparticle morphology and polydispersity.

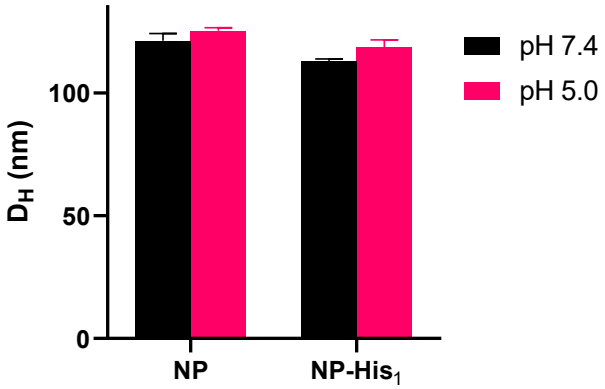

Supplementary Figure S8. Dynamic Light Scattering analysis shows NP and NP-His_1-EG_8 have similar size, with minimal change upon change in pH.

Supplementary Table S2. Dynamic Light Scattering analysis of NP and TNP loaded with 0-2% His_n-EG_8 and 0% (NP) or 1% (TNP) targeting peptide. Measurements performed at pH 7.4. Minimal size variation and low polydispersity is observed across all formulations.

	Non-Targeted Nanoparticles		**Targeted Nanoparticles**	
	Eff. Diameter (nm)	**PD**	**Eff. Diameter (nm)**	**PD**
0%	118.6±1.3	0.07±0.04	117.0±3.2	0.11±0.06
His_1-EG_8				
0.25%	119.7±1.5	0.09±0.06	117.0±1.5	0.07±0.04
0.5%	118.6±3.1	0.15±0.05	117.7±3.6	0.07±0.07
1%	118.7±1.6	0.02±0.00	118.9±1.9	0.08±0.03
2%	117.9±3.2	0.05±0.04	113.2±1.0	0.04±0.02
His_3-EG_8				
0.25%	113.5±2.1	0.08±0.04	119.2±2.0	0.07±0.03
0.5%	115.6±2.7	0.08±0.09	121.6±1.9	0.07±0.03
1%	123.0±2.4	0.05±0.06	117.0±0.8	0.06±0.03
2%	126.2±3.9	0.06±0.06	133.1±3.2	0.11±0.03
His_{10}-EG_8				
0.25%	111.7±2.9	0.06±0.04	116.6±2.3	0.09±0.05
0.5%	117.7±2.5	0.03±0.02	115.6±2.5	0.06±0.03
1%	119.3±1.6	0.06±0.03	120.2±3.6	0.10±0.04
2%	124.8±1.2	0.06±0.04	120.6±1.7	0.11±0.05

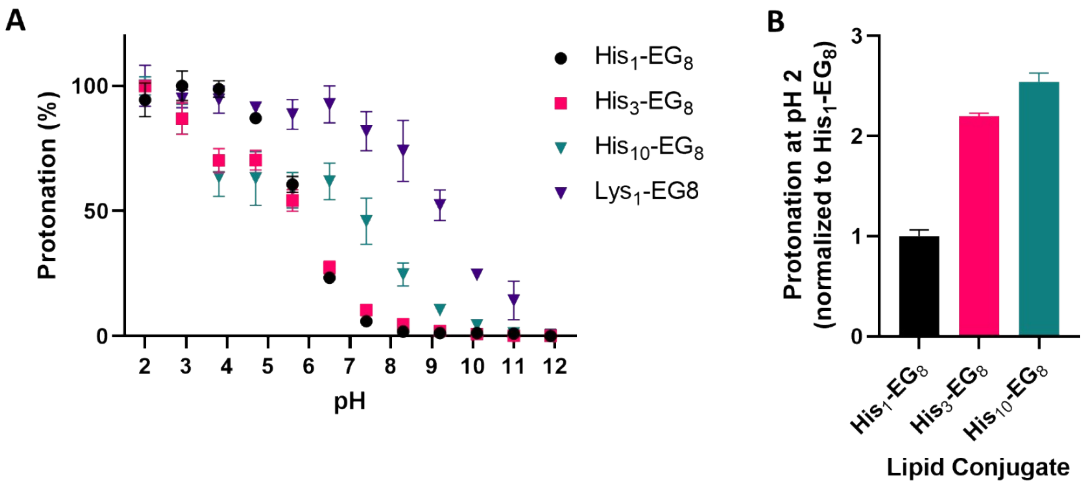

Supplementary Figure S9. (A) TNS Protonation assay for His_n-EG_8 shows a pK_a of ~5.8 for His_1-EG_8, ~5.7 for His_3-EG_8 and at least two distinct pK_a's for His_{10}-EG_8 (estimated at pH ~3 and ~7.4). Lys_1-EG_8 lipid conjugate (pKa ~9.6) was evaluated side-by-side to confirm accuracy of the assay. (B) Total protonated groups of His_n-EG_8 lipid conjugates normalized to His_1-EG_8 show inefficient protonation of long oligohistidine chains such as His_{10}-EG_8. Bars and markers represent mean ±S.D. of triplicates.

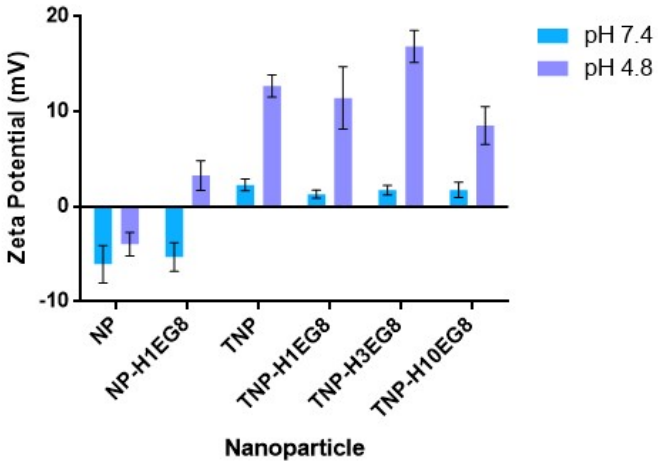

Supplementary Figure S10. Zeta potential analysis of NP and TNP with and without His_n-EG_8 was performed at pH 7.4 and 4.8 as described in the materials and methods section. The targeting peptide for these experiments was 1% LPAM1pep. Bars represent mean ± S.D. of n>5 readings.

Supplementary Table S3. NP and TNP were loaded with 166, 500 or 1500 histidine residues per particle. Table shows equivalent %mol for each His_n-EG_8 conjugate.

His residues	His_1 (%mol loading)	His_3 (%mol loading)	His_{10} (%mol loading)
166	0.21%	0.07%	0.02%
500	0.64%	0.21%	0.06%
1500	1.87%	0.64%	0.19%

Supplementary Table S4: Spatial distribution of lipid conjugates. Liposomal area and the total number of lipids per liposomal nanoparticle were first calculated assuming a spherical liposome. The spacing between each peptide-lipid conjugated is calculated from the ligand density assuming evenly spaced ligands in a square grid. *The number of lipid conjugates considers only the outer leaflet of the liposome.

Diameter (nm)	Lipid Conjugate (%mol loading)	Liposome Area (nm^2)	Lipids per Liposome	Total Lipid Conjugates*	Lipid Conjugate Density (nm^2/conjugate)	Distance between conjugates (nm)
100	0.25	31,415.93	80,092.5	100.1	313.8	17.7
100	0.5	31,415.93	80,092.5	200.2	156.9	12.5
100	1	31,415.93	80,092.5	400.5	78.4	8.8
100	2	31,415.93	80,092.5	800.9	39.2	6.3

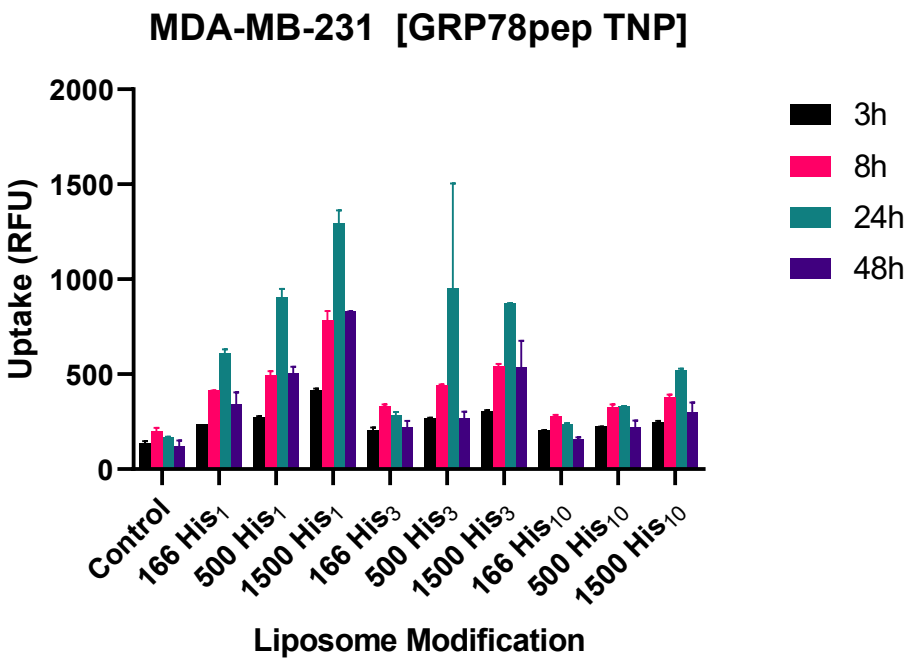

Supplementary Figure S11. Cellular uptake of GRP78pep TNP on metastatic triple negative breast cancer cell line MDA-MB-231. Internalization is depends on His_n chain length, total number of His and incubation time.

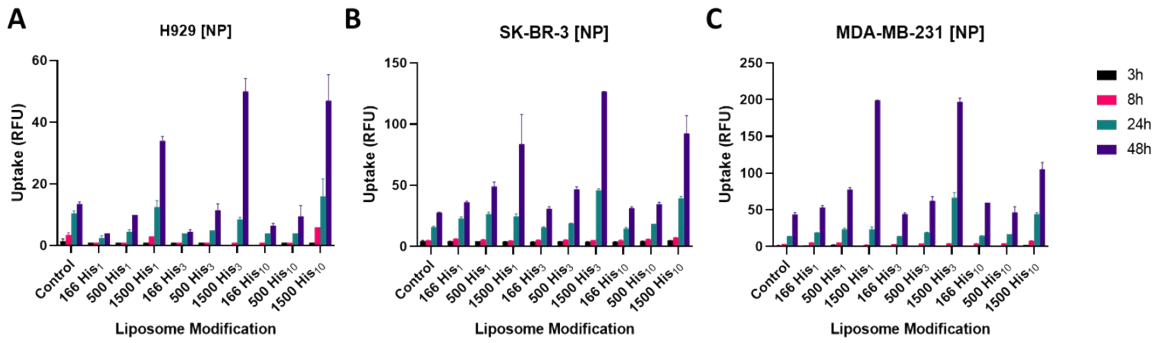

Supplementary Figure S12. Cellular uptake of non-targeted NP on H929 and MBA-MB-231 cell lines. At high concentrations of His_n cellular internalization is triggered.

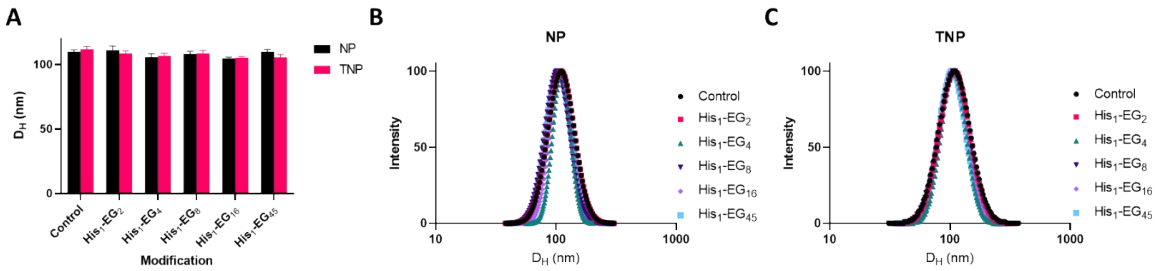

Supplementary Figure S13. Dynamic Light Scattering evaluation of NP and TNP loaded with His_1-EG_m lipid conjugates where m=2-45 show minimal differences in nanoparticle size.

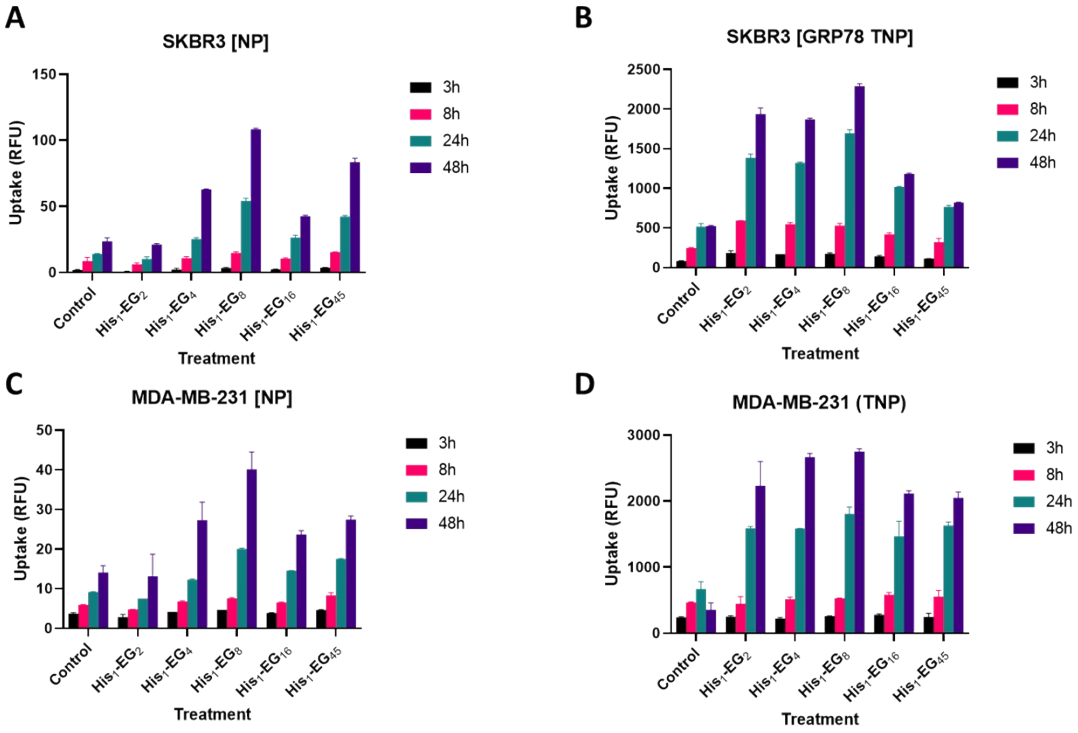

Supplementary Figure S14. Evaluation of His_1-EG_m-loaded NP and TNP on SKBR3 and MDA-MB-231 cell lines show different trends in NP and TNP. No trend was easily detectable for NP, while internalization of TNP benefited from shorter EG linkers.

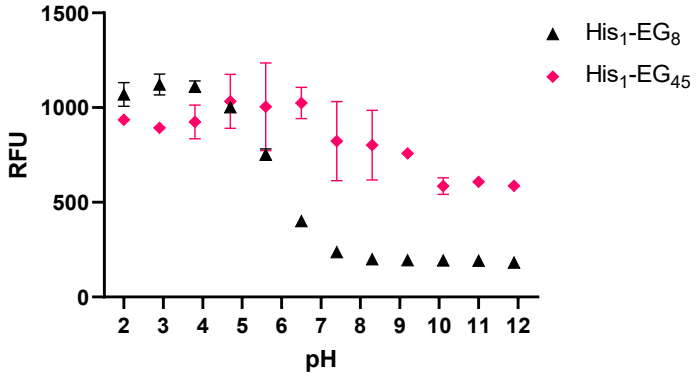

Supplementary Figure S15. TNS protonation assay of His_1-EG_8 and His_1-EG_{45} shows abnormal protonation pattern of His_1-EG_{45}.

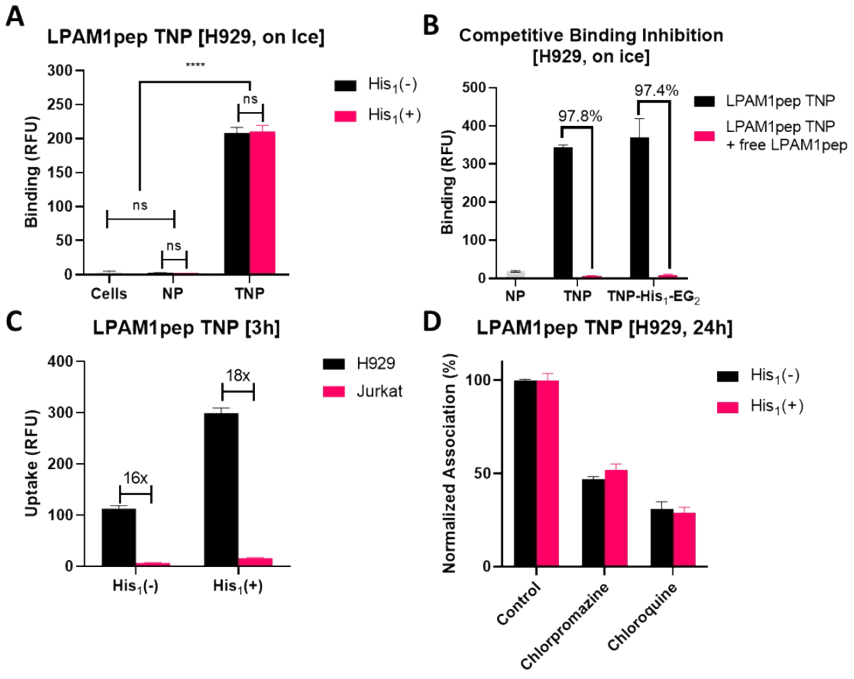

Supplementary Figure S16. (A) Addition of His_1-EG_2 does not affect cell surface binding or NP or TNP. (B) Receptor-specificity of TNP binding was evaluated by competitive inhibition with free peptide. (C) Selectivity of the treatment was maintained when comparing internalization by H929 (LPAM1+) or Jurkat (LPAM1-) cell lines. (D) Effect of endocytosis inhibitors chlorpromazine and chloroquine on TNP cellular internalization.

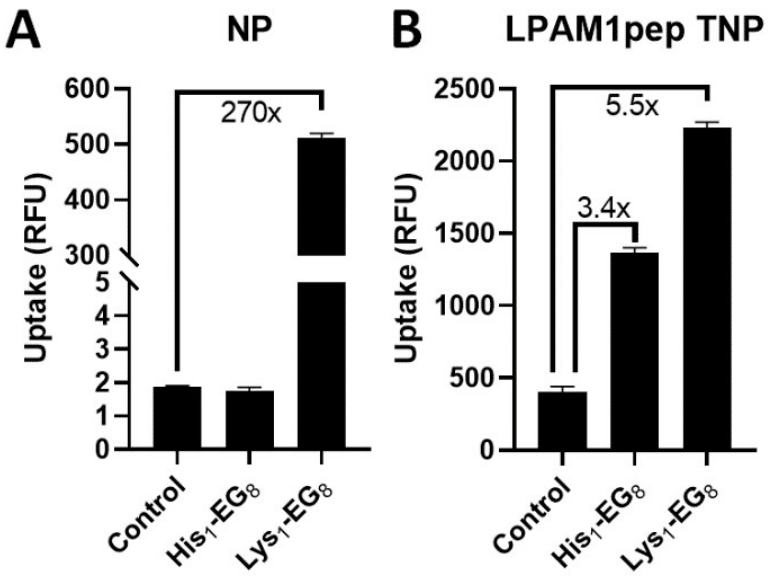

Supplementary Figure S17. Cellular internalization of NP (A) and LPAM1pep-TNP (B) containing His_1-EG_8 or Lys_1-EG_8 was evaluated on H929 cells. While both conjugates provide advantages in TNP internalization, His_1-EG_8 does not produce non-specific cellular internalization of NP.

Supplementary Table S5. Name, targeted receptor, primary sequence and reference for all targeting peptides evaluated.

Peptide	Target	Sequence	Reference
LPAM1pep	LPAM-1 ($\alpha_4\beta_7$ integrin)	CRSDTLCGE	Dubree et al, 2002[48]
VLA4-pep	VLA-4 ($\alpha_4\beta_1$ integrin)	YCDPC	Jackson et al, 1997[63]
CD138pep	CD138 (Syndecan-1)	RKRLQVQLSIRT	Hayashi et al, 2002[65]
CD38pep	CD38	ARGDYYGSNSLDYW	Omstead et al, 2020[64]

HER2pep	HER2/neu	YCDGFYACYMDV	Berezov et al, 2001[66]
LRP1pep	LRP1	TFFYGGSRGKRNNFKTEEY	Demuele et al, 2007[67]
GRP78pep	GRP78	SNTRVAP	Mandelin et al, 2015[49]
iRGD	$\alpha_V\beta_3$, $\alpha_V\beta_5$	CRGDKGPDC	Sugahara et al, 2009[68]

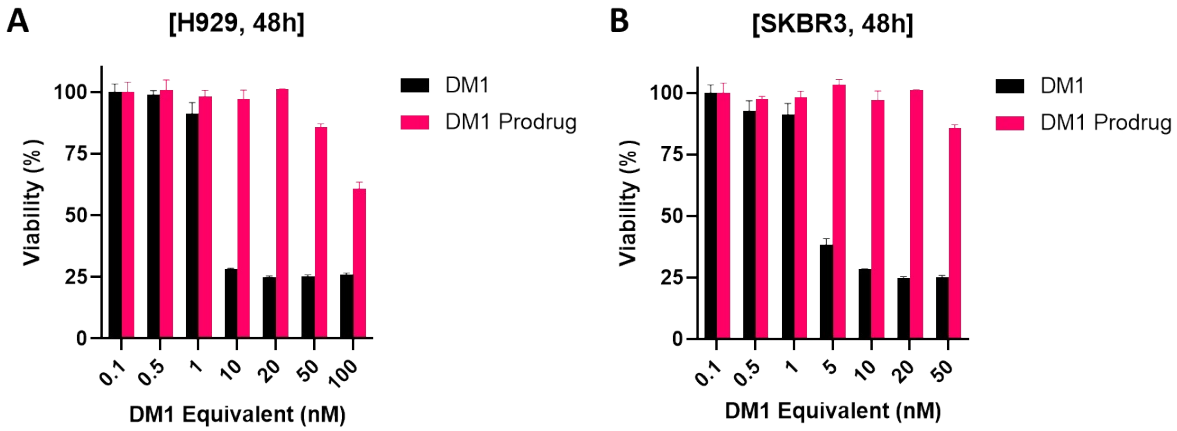

Supplementary Figure S18. Cytotoxicity of DM1 and DM1 prodrug on H929 and SKBR3 cell lines was evaluated. 48h after dosing, CCK8 solution was added to each treatment well for analysis of cell viability.

Supplementary Table S6. Loading efficiency of DM1 Prodrug in TNP and TNP-His_1-EG_2

	LPAM1pep Loading	**His1-EG2 Loading**	**Prodrug Loading**
TNP[DM1]	95.4%	N/A	95.5%
TNP-His_1-EG_2[DM1]	97.1%	97.5%	95.6%

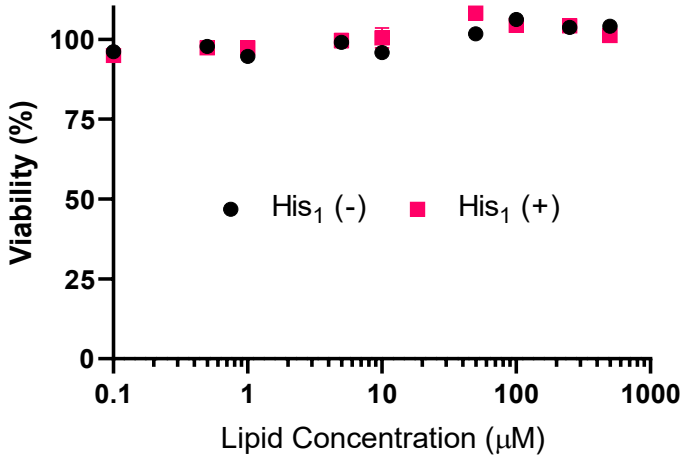

Supplementary Figure S19. Cytotoxicity assay of His_1(-) and His_1(+) nanoparticles on H929 cells shows these particles are not toxic in the absence of chemotherapeutic agents.

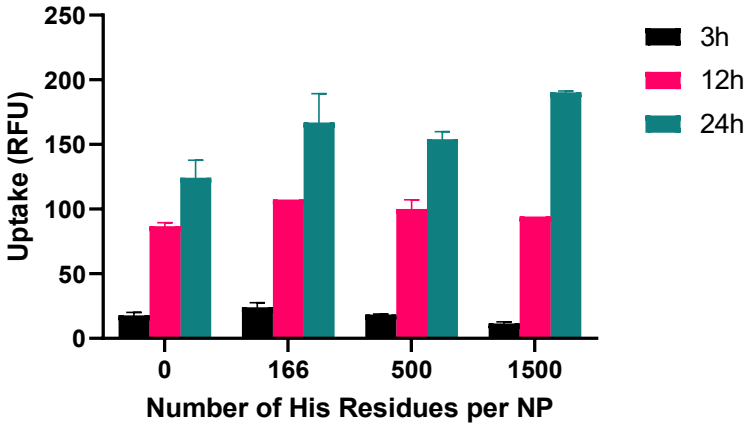

Supplementary Figure S20. Flow cytometry analysis of the interaction between His_1-EG_2-NP and bone marrow-derived macrophages (BMDM) shows minimal increase in cellular uptake.